Journal of
Composites Science

MDPI

Article

Development, Dielectric Response, and Functionality of $ZnTiO_3/BaTiO_3$/Epoxy Resin Hybrid Nanocomposites

Anastasios C. Patsidis [1,*], Eleftherios I. Koufakis [1], Georgios N. Mathioudakis [2], Orestis Vryonis [1,3] and Georgios C. Psarras [1,*]

[1] Smart Materials & Nanodielectrics Laboratory, Department of Materials Science, School of Natural Sciences, University of Patras, 26504 Patras, Greece; lekouf@hotmail.com (E.I.K.); o.vryonis@soton.ac.uk (O.V.)
[2] Institute of Chemical Engineering Sciences (ICE-HT), Foundation for Research & Technology-Hellas (FORTH), Stadiou Str., Platani, P.O. Box 1414, 26504 Patras, Greece; mathioy@iceht.forth.gr
[3] Tony Davies High Voltage Laboratory, Department of Electronics and Computer Science, Faculty of Engineering and Physical Sciences, University of Southampton, Southampton SO17 1BJ, UK
* Correspondence: patsidis@upatras.gr (A.C.P.); g.c.psarras@upatras.gr (G.C.P.); Tel.: +30-2610-997835 (A.C.P.); +30-2610-996316 (G.C.P.)

Abstract: In the present work, hybrid nanocomposites of an epoxy resin reinforced with $ZnTiO_3$ and $BaTiO_3$ nanoparticles, at various filler contents, were fabricated and studied. The successful integration of ceramic nanofillers and the fine distribution of nanoparticles were confirmed via X-ray Diffraction patterns and Scanning Electron Microscopy images, respectively. Dielectric properties and related relaxation phenomena were investigated via Broadband Dielectric Spectroscopy in a wide range of frequencies and temperatures. Data analysis showed that dielectric permittivity increases with filler content, although optimum performance does not correspond to the maximum $ZnTiO_3$ content. Four relaxation processes were observed and attributed to interfacial polarization (IP) (at low frequencies and high temperatures), glass-to-rubber transition (α-relaxation) of the epoxy matrix (at intermediate frequencies and temperatures), and local rearrangements of polar side groups of the macromolecules (β-relaxation) and small flexible groups of the main polymer chain (γ-relaxation) occurring at low temperatures and high frequencies. The ability of hybrid nanocomposites to store and retrieve energy was studied under dc conditions by employing a charging/discharging sequence. The stored and retrieved energy increases with filler content and charging voltage. The optimum ability of energy recovering, shown by the epoxy/7 phr $ZnTiO_3$/7 phr $BaTiO_3$ nanocomposite, ranges between 30 and 50 times more than the matrix, depending on the time instant. The employed nanoparticles induce piezoelectric properties in the nanocomposites, as found by the increase in the piezoelectric coefficient with filler content.

Keywords: hybrid polymer nanocomposites; dielectric properties; relaxations; energy storing/retrieving; piezoelectric properties

Citation: Patsidis, A.C.; Koufakis, E.I.; Mathioudakis, G.N.; Vryonis, O.; Psarras, G.C. Development, Dielectric Response, and Functionality of $ZnTiO_3/BaTiO_3$/Epoxy Resin Hybrid Nanocomposites. *J. Compos. Sci.* **2024**, *8*, 225. https://doi.org/10.3390/jcs8060225

Academic Editor: Chensong Dong

Received: 10 April 2024
Revised: 21 May 2024
Accepted: 12 June 2024
Published: 15 June 2024

1. Introduction

Nowadays, the scientific and technological impact of polymer matrix nanocomposites (PNCs) is well established [1–3]. Polymer matrix composites and especially fibrous systems became an important class of engineering materials because of their mechanical properties, lightweight nature, thermal stability, and the adaptation of complex shapes and forms [1,2]. By these means, they are employed as structural components in industrial applications in the fields of automobiles, aerospace, naval engineering, civil engineering, and others. The era of nanostructured materials gave an additional impetus to polymer matrix composites. By employing a nano-scaled reinforcing phase, such as nanoparticles, nanofibers, or nanoflakes, the interfacial area enhances significantly and the PNCs' response is governed not only by the properties of the constituents but also by the occurring interactions at the

interface [4,5]. In this context, nanofiller appears as a dispersive phase and besides the mechanical properties, thermal, electrical and magnetic responses are attracting attention and acquire significance [6–15]. The next step, which is currently considered as the focal point of cutting-edge research, is the development of multifunctional PNCs. Multifunctional performance can be defined as the combination of various desirable properties or behaviors in a single materials' system. The multitasking system is able to respond differently depending upon the type of loading conditions or signal control, which activate the relative properties each time. Thus, the mechanical, thermal, electrical, and magnetic response can be triggered and tuned by controlling the type and the amount of reinforcing phase or phases [7,11–14]. Hybrid PNCs have the advantage of modulating complementary properties/responses and interactions of the reinforcing phases and the matrix material [11–14]. Ceramic nanofillers, such as carbon nano-forms, influence both the mechanical properties and the conductivity of PNCs, while ferrite nanoparticles integrate magnetic performance to nanosystems. Polar oxides augment the dielectric permittivity and the electrical energy storage of PNCs, while ferroelectric and/or piezoelectric crystal particles exhibit a high level of adjustable polarization via their thermally induced phase/structural changes, thus providing an additional side of multitasking performance [13–17]. The properties of ceramic-filler/PNCs can be exploited in plenty of applications, including integrated decoupling capacitors, acoustic emission sensors, angular acceleration accelerometers, remote energy storing devices, and leakage current controllers [1–3,11,14].

In this study, hybrid nanocomposites of epoxy resin and ceramic nanoparticles of zinc titanate ($ZnTiO_3$) and barium titanate ($BaTiO_3$) were prepared and studied, for the first time, at various concentrations of the reinforcing phases. $BaTiO_3$ is a well-known polymorphic ferroelectric material, undergoing structural phase transition from the orthorhombic to the tetragonal phase at ~5–40 °C (depending on the single crystal or polycrystalline structure of the sample) and from the tetragonal to the cubic structure at ~130 °C. At this temperature, which is known as Curie temperature, $BaTiO_3$ switches from the non-symmetrical, polar structure to the symmetrical, non-polar one. Curie temperature varies with the single-crystal or ceramic type of barium titanate and the size of crystal particles. The extent of the ferroelectric to paraelectric transition has been found to depend on the aspect ratio of the unit cell dimensions. As the aspect ratio approaches unity, the unit cell's tetragonality decreases, causing a reduction in the polar ferroelectric phase below the Curie temperature [16–18]. $ZnTiO_3$ is a dielectric material prepared via a typical solid-state reaction between ZnO and TiO_2, resulting in three possible forms ($ZnTiO_3$, Zn_2TiO_4, $Zn_2Ti_3O_8$) [6,19–21]. The ferroelectric to paraelectric transition of perovskite-type zinc titanate has been reported, with highly deviating Curie temperatures (5 or 455 °C), according to the size of the $ZnTiO_3$ particles (micro or nano) and the preparation method (solid-state reaction or hydrothermal synthesis) [22,23]. In addition, the piezoelectric properties of $ZnTiO_3$ nanocrystals acquire engineering importance, since they can be exploited as the converting interface of mechanical stimuli (human steps, acoustic waves, vibrations, fluid flow, etc.) to electricity. Integrating piezoelectric nanoparticles in bulk polymer matrices or polymer films results in the formation of nano-scaled devices, where piezoelectric particles act as nanogenerators by coupling mechanical with electric energy [23,24]. The development of hybrid PNCs, by integrating two different polar reinforcing phases, is expected to influence their dielectric response and the resulting piezoelectric properties. In this study, the employed $ZnTiO_3$ was in its perovskite structure. The used polymer matrix was a typical bisphenol-A epoxy resin, selected for its thermomechanical stability, low shrinkage, ease of processing and workability, and low cost. The successful integration of nanoparticles was checked via X-ray Diffraction (XRD) patterns. The morphology of the fabricated hybrid nanocomposites and the fine distribution of the nanofiller was assessed by Scanning Electron Microscopy (SEM) images. Differential Scanning Calorimetry (DSC) was used for the determination of the glass transition temperature (T_g). The dielectric properties and the related relaxation phenomena were studied by means of Broadband Dielectric Spectroscopy (BDS) in the temperature range from −100 °C to 160 °C and fre-

quency range from 10^{-1} Hz to 10^{7} Hz. Data analysis was conducted in terms of dielectric permittivity and electric modulus formalisms as a function of temperature, frequency, and the fillers' concentration. The ability of the fabricated hybrid nanocomposites to store and retrieve electric energy was investigated under dc conditions by employing a charging–discharging sequence of the specimens, varying the charging voltage and the fillers' content as a function of time. Finally, the piezoelectric properties of the hybrid systems were investigated via the determination of the piezoelectric coefficient d_{33} under time-varying exerted mechanical stress.

2. Materials and Methods

A low-viscosity epoxy resin (Epoxol 2004 A), and a slow rate hardener (Epoxol 2004 B) were employed as the matrix materials. Both ingredients were provided by Neotex S.A. Athens, Greece. The epoxy prepolymer was diglycidyl ether of bisphenol-A (DGEBA), while the hardener was an aromatic diamine. $ZnTiO_3$ and $BaTiO_3$ nanopowders, both provided by Sigma-Aldrich(St. Louis, MO, USA), were used as the reinforcing phases. The employed nanoparticles were spheroids with a diameter less than 100 nm in the case of $ZnTiO_3$ and 30 to 50 nm for $BaTiO_3$. For the fabrication of the specimens, epoxy resin and the curing agent were mixed at a 2:1 (w/w) mass ratio and then loaded with precalculated amounts of reinforcing nanoparticles in order to obtain the required filler contents. The produced mixtures were stirred at a low rate and sonicated to obstruct the formation of agglomerates and to achieve a fine particle distribution. After degassing, the mixtures were poured into suitable silicon molds. Specimens were cured in ambient conditions for a week and then post-cured at 100 °C for four hours. The obtained specimens were in the form of circular disks with a 30 mm diameter and an average thickness of 1.5 mm. The concentration of zinc titanate and/or barium titanate in the hybrid nanocomposites was 3, 5, and 7 parts per hundred resin per weight (phr), resulting in nine different systems. For comparison reasons, a neat epoxy specimen and binary composites with either $ZnTiO_3$ or $BaTiO_3$ nanoparticles were also prepared.

The morphological and structural characterization of the prepared nanocomposites was conducted by means of Scanning Electron Microscopy (SEM) images and X-ray Diffraction (XRD) patterns. SEM images were obtained via an EVO MA 10 Zeiss SEM microscope operating at 15.75 kV, while samples were coated via sputtering with a 10 nm layer of Au, prior to imaging, to eliminate charging. For the XRD patterns, a Philips PW 1050/25 goniometer and Cu Ka X-ray radiation (λ = 1.5418 Å) were employed.

Thermal analysis of the hybrid nanosystems was conducted via Differential Scanning Calorimetry (DSC) with a TA Q800 DSC calorimeter at heating rate of 10 °C/min. Examined samples were shielded in aluminum crucibles, and an empty identical crucible was used as the reference. The glass transition temperature was determined by the point of inflexion of the recorded endothermic transition of heat capacity in the thermographs. For this reason, suitable software supplied by TA Instruments (New Castle, DE, USA)was used. The determined values for T_g are listed in Table 1.

The electrical response of all the fabricated systems was carried out using Broadband Dielectric Spectroscopy (BDS) via an Alpha-N frequency response analyzer. Specimens were put in a parallel plate configuration in BDS 1200 dielectric cell between gold-plated electrodes. Measurements were conducted in a frequency range from 0.1 Hz to 10 MHz, under isothermal conditions, with V_{rms} = 1 V and a temperature step of 10 °C. Temperature was controlled via a Quatro system between −100 and 160 °C. Data recording was conducted in real time via WinDeta software. The experimental setup and employed software for electrical measurements were all supplied by Novocontrol Technologies (Montabaur, Germany). Electrical studies were executed according to the ASTM D150 [25] specifications.

Table 1. Nanocomposites' filler content, glass transition temperature as determined via DSC, and parameters of molecular dynamic analysis as obtained by fitting relaxations via Equations (1) and (2).

Filler Mass Fraction $ZnTiO_3/BaTiO_3$ (phr)	T_g (°C)	IP E_A (eV)	γ-Relaxation E_A (eV)	α-Relaxation B (K)	T_V (K)
0 (neat epoxy)	58.90	0.588	0.614	802.66	265.44
5/0	52.35	0.789	0.670	625.85	272.44
0/5	60.29	0.591	0.648	686.68	272.44
5/3	56.60	0.718	0.701	630.35	276.44
3/5	46.43	0.542	0.676	609.65	276.44
5/5	43.95	0.665	0.669	546.43	282.6
7/5	49.20	0.876	0.662	474.75	286.56
5/7	65.34	0.597	0.669	474.95	286.44

The energy storing/retrieving ability of hybrid nanocomposites was investigated by measuring, in real time, the charging and discharging currents under dc conditions, via a High-Resistance Meter 4339B dc device supplied by Agilent. Specimens were put between the electrodes of a parallel plate capacitor and then were charged by applying an external dc voltage. The charging current was recorded as a function of time for 60 s. Right afterwards the charging voltage was turned off, the discharging current was recorded again as a function of time. Before any test sequence, a discharging short-circuit procedure was exerted to eliminate the possible presence of previously stored charges in the specimens. All charging/discharging tests were conducted according to the ASTM D257 [26] specifications at ambient. The analytical description of the energy storing/retrieving tests has been given previously [8,17].

Finally, the piezoelectric measurements were carried out via a Piezometer Tester (Piezometer System PM300) supplied by Piezotest (London, UK). The applied stress stimulus was varying harmonically with a frequency of 110 Hz, while the force amplitude was 0.25 N.

3. Results

Figure 1 presents representative SEM images of the hybrid nanocomposites with filler content: (a) 3 phr nano-$ZnTiO_3$/3 phr nano-$BaTiO_3$; (b) 7 phr nano-$ZnTiO_3$/7 phr nano-$BaTiO_3$. Examination of the cryo-fractured surfaces of the studied specimens reveals fine dispersion of the employed nanoparticles in the epoxy resin even at the highest filler content and the absence of extensive agglomerates and voids. Nanodispersions can easily be observed in all cases. Figure S1 presents a cross-sectional cryo-fractured surface for the epoxy/7 phr nano-$ZnTiO_3$/7 phr nano-$BaTiO_3$ nanocomposite at a lower magnification.

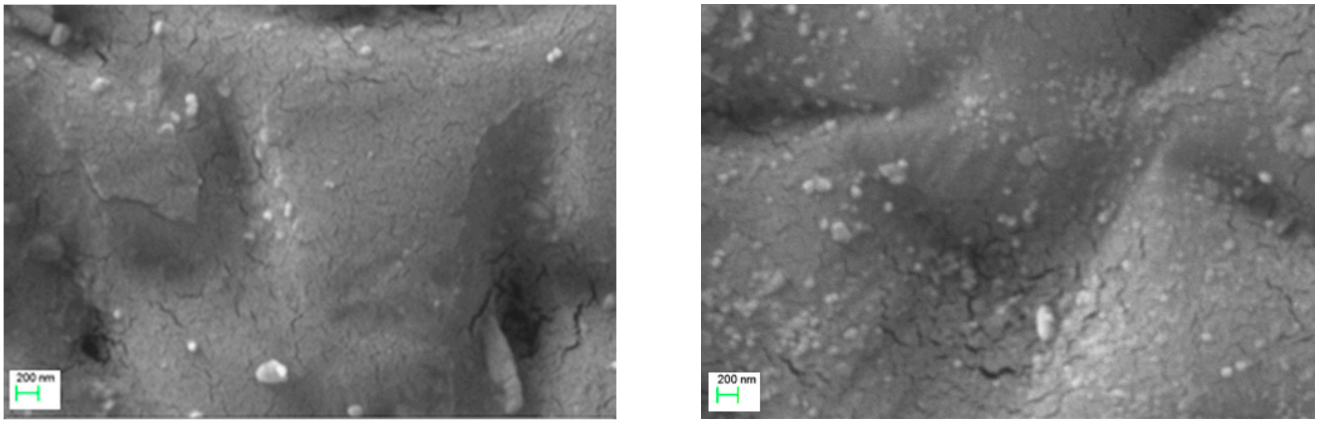

(**a**) (**b**)

Figure 1. Representative SEM images for the nanocomposites: (**a**) epoxy/3 phr $ZnTiO_3$/3 phr $BaTiO_3$ and (**b**) epoxy/7 phr $ZnTiO_3$/7 phr $BaTiO_3$.

The XRD patterns of the $ZnTiO_3$ and $BaTiO_3$ nanopowders are depicted in Figure 2a. The characteristic peaks of the cubic phase of $BaTiO_3$ are shown at 23.0, 32.2, 39.5, 45.8, 51.5, 56.8, 66.5, 71.0, and 75.5º at 2θ angle, which correspond to the (100), (101), (110), (200), (210), (202), (212), and (310) planes. Concerning the pattern of $ZnTiO_3$, the following peaks, 30.7, 36.0, 43.5, 53.7, 57.3, 62.8, and 72.1°, are detectable, corresponding to the (104), (110), (113), (116), (211), (440), and (201) planes, which are indicative for the hexagonal perovskite structure. Figure 2b depicts the XRD patterns of unreinforced resin and hybrid nanocomposites. The thermosetting matrix gives a characteristic halo commonly observed in the amorphous resins. The XRD diffractograms of the epoxy resin composites with $ZnTiO_3$ and $BaTiO_3$, at varying percentages, exhibit the characteristic peaks of both fillers along with the halo peak of the resin. It is noticeable that the different percentage of the $ZnTiO_3$ or $BaTiO_3$ is imprinted on the intensities of the characteristic XRD peaks.

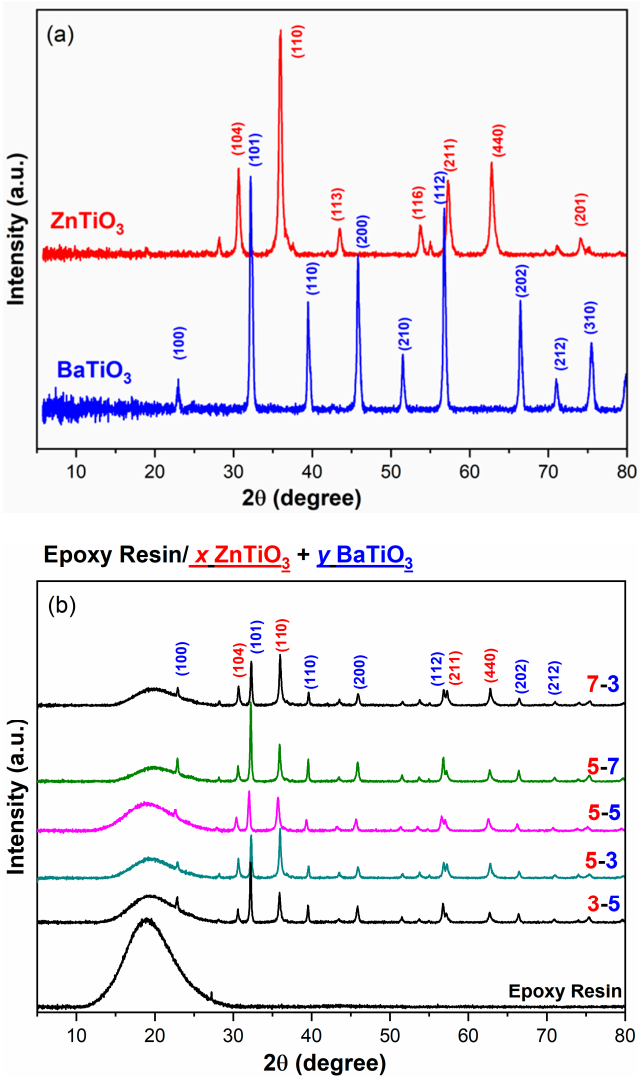

Figure 2. XRD patterns of (**a**) the employed nanoparticles and (**b**) the neat epoxy resin and the fabricated hybrid nanocomposites.

Characteristic 3D diagrams of the dielectric response of the examined nanocomposites are depicted in Figures 3 and 4 (for the nanocomposites epoxy/3 phr nano-$ZnTiO_3$/3 phr nano-$BaTiO_3$ and epoxy/7 phr nano-$ZnTiO_3$/7 phr nano-$BaTiO_3$, respectively), where the dielectric spectra of the real part of dielectric permittivity (ε') and the loss tangent ($\tan\delta$) are shown as a function of temperature and frequency. In Figures 3a and 4a, ε' attains high values with diminishing frequency and increasing temperature. As expected, in the

low-frequency and high-temperature region, dipoles (permanent and induced) acquire sufficient time to be aligned with the field, while thermal agitation further facilitates their orientation. This a typical behavior for PNCs and it has been reported several times [6,11,13,14]. Permittivity values diminish with frequency because dipoles cannot follow the fast alternation of the field. In the temperature range from 20 to 120 °C, a transition from high to low values is recorded for all the examined systems, which appears as a "step". This process is attributed to the glass-to-rubber transition of the epoxy matrix and is also evident in the neat matrix spectra (Figure S2). It should be noted that no evidence for the ferroelectric behavior of $ZnTiO_3$ was detected in the DSC thermographs or the isochronal dielectric plots (0.1 Hz) of nanoparticles and nanocomposites. Figure S3 presents isochronal plots of (ε') versus temperature for $ZnTiO_3$ nanopowder and hybrid nanocomposites.

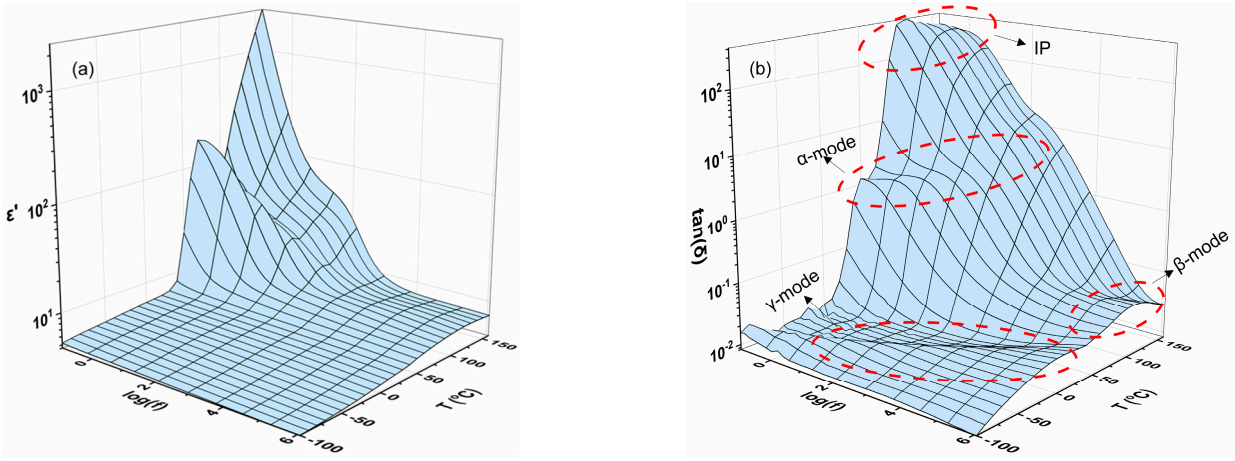

Figure 3. (**a**) Real part of dielectric permittivity and (**b**) loss tanδ as a function of frequency and temperature for the epoxy/3 phr $ZnTiO_3$/3 phr $BaTiO_3$ nanocomposite.

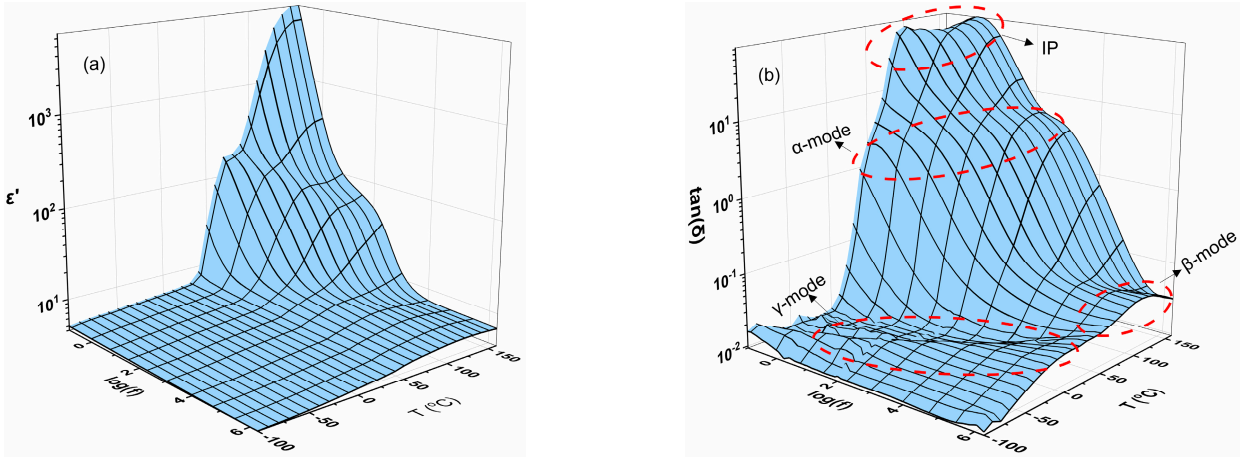

Figure 4. (**a**) Real part of dielectric permittivity and (**b**) loss tanδ as a function of frequency and temperature for the epoxy/7 phr $ZnTiO_3$/7 phr $BaTiO_3$ nanocomposite.

The loss tangent spectra in Figures 3b and 4b, for the same hybrid systems as previously, include four distinct relaxation processes, which become apparent via the formation of loss peaks. From the low- to the high-frequency region, the relaxations are ascribed to interfacial polarization (IP), also known as Maxwell–Wagner–Sillars phenomenon, glass-to-rubber transition (denoted as α-relaxation), local reorientation of small polar side groups of the main macromolecular chain (denoted as β-relaxation), and rearrangement ("crankshaft rotation") of small flexible parts of the main polymer chain (denoted as γ-relaxation). The

IP and α-process are characterized by longer relaxation times, while the local motions of the β- and γ-processes are faster, corresponding to shorter relaxation times.

4. Discussion

Aiming to examine the effect of the content of each reinforcing phase upon the dielectric properties, the spectra of the real part of dielectric permittivity and the imaginary part of the electric modulus (loss modulus index, M″) are presented isothermally versus frequency, by keeping constant each time the content of a specific filler and varying the other. Figure 5a,b present the ε′ vs. log*f* spectra at −50 and 20 °C, respectively, for the nanocomposites with a constant content of $ZnTiO_3$ at 5 phr and varying the $BaTiO_3$ content. Hybrid systems exhibit higher values of the real part of dielectric permittivity, with respect to the matrix, in the whole frequency range in both temperatures. Moreover, ε′ augments with the increase in the $BaTiO_3$ content. This behavior is attributed to the high values of permittivity of barium titanate [8,16,27]. In Figure 6a,b, ε′ as a function of frequency at −50 and 20 °C is shown for the systems with a constant $BaTiO_3$ content at 5 phr and varying the $ZnTiO_3$ content. Although the general trend in the spectra is the same as that of Figure 5, it should be noted that the system with the higher $ZnTiO_3$ content does not attain the maximum values of ε′. Apparently, the optimum response does not correspond to the higher $ZnTiO_3$ content.

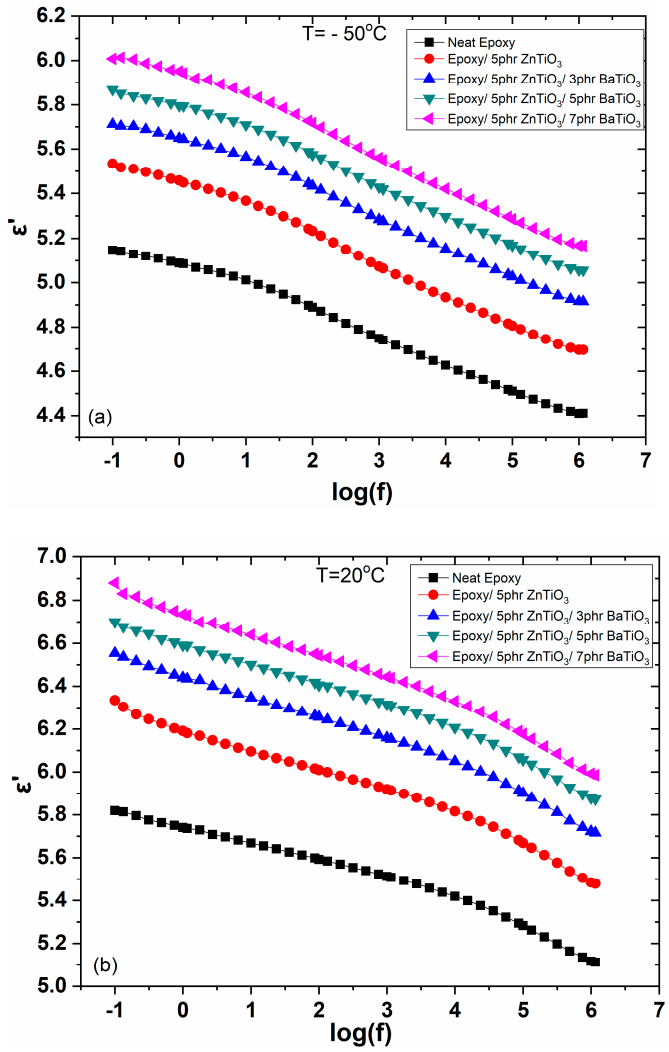

Figure 5. The real part of dielectric permittivity as a function of frequency for the systems epoxy/5 phr $ZnTiO_3$/x phr $BaTiO_3$ at (**a**) −50 °C and (**b**) 20 °C.

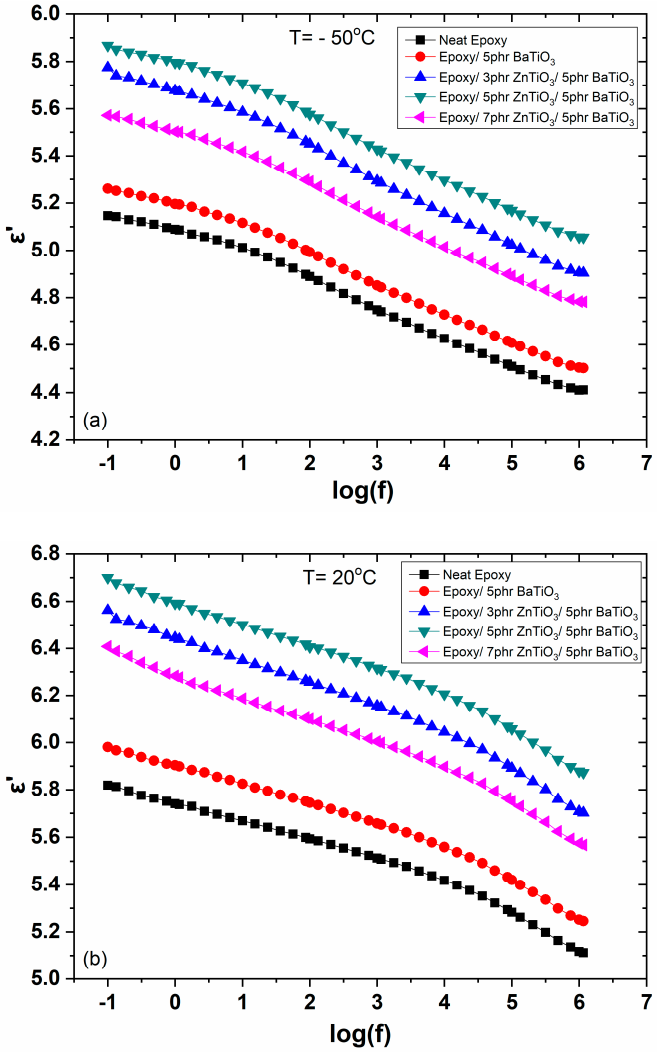

Figure 6. The real part of dielectric permittivity as a function of frequency for the systems epoxy/x phr $ZnTiO_3$ phr/5 phr $BaTiO_3$ at (**a**) −50 °C and (**b**) 20 °C.

Figure 7 depicts α-relaxation in the form of loss modulus peaks, at 50 °C, as a function of frequency. This type of graph can be employed for studying the occurring interaction between filler and macromolecules [4,13,28]. In the case that the glass-to-rubber transition shifts to higher frequencies, under isothermal conditions, by increasing the filler content, there is a clear indication that T_g decreases because of weak interactions between nanoparticles and polymer chains [4,28]. In the opposite case, by shifting the α-loss peak to lower frequencies, at a constant temperature, with the increase in the reinforcing phase, the glass transition temperature increases due to the strong interactions between the filler and polymer matrix, which leads to a reduction in the chains' mobility. Thus, large parts of the polymer chains, in the thermosetting matrix, can relax simultaneously only if a higher thermal agitation is provided [4,28]. Figure 7a presents the α-loss peaks for the hybrid systems with a constant $ZnTiO_3$ content (5 phr) and varying the $BaTiO_3$ content. Interestingly, the loss peak of the nanocomposite with only zinc titanate filler shifts to higher frequencies with respect to the neat epoxy matrix, while as the content of barium titanate increases, the α-loss peak moves backwards to lower frequencies. Figure 7a indicates that the $ZnTiO_3$/epoxy interactions can be considered as relatively weak and the $BaTiO_3$/epoxy interactions as relatively strong. The same trend is observed in Figure 7b, where the isothermal loss modulus spectra versus frequency show that the peak of the 5 phr $BaTiO_3$/epoxy binary system shifts to lower frequencies relative to the unreinforced

epoxy, while as the content of $ZnTiO_3$ augments, peaks follow the opposite direction to higher frequencies. These results are further supported by Figure S5, where the variation in the α-loss peak for binary $ZnTiO_3$/epoxy and $BaTiO_3$/epoxy nanocomposites is given. It can be easily seen that the increase in zinc titanate shifts the glass-to-rubber transition loss peak to higher frequencies, while the opposite trend is recorded when the barium titanate concentration alters.

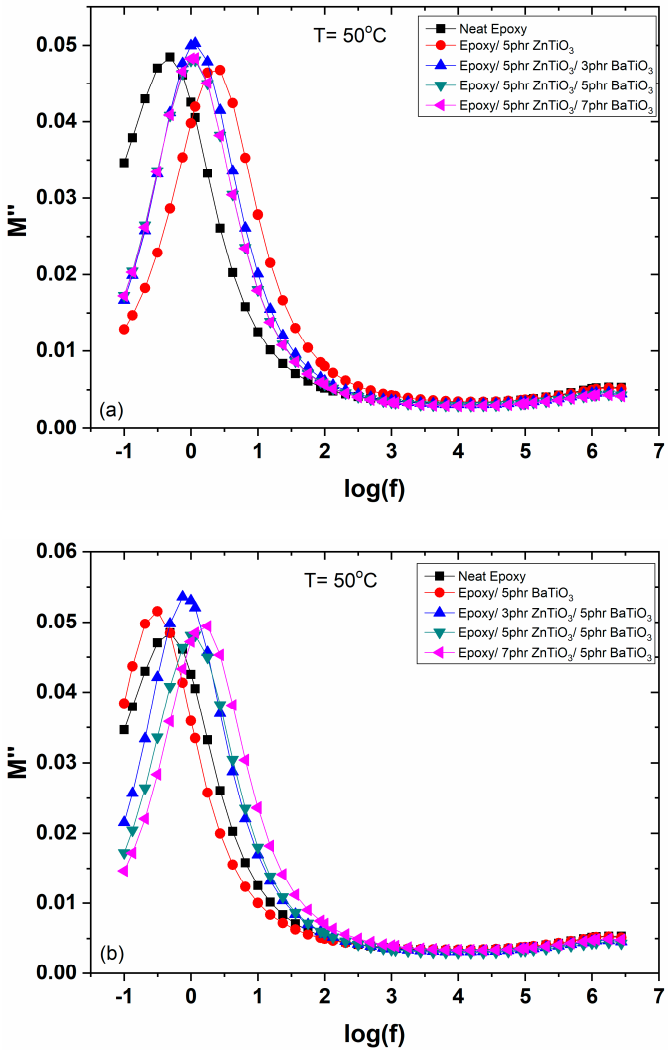

Figure 7. Imaginary part of electric modulus as a function of frequency at 50 °C for the nanocomposites: (**a**) epoxy/5 phr $ZnTiO_3$ phr/x phr $BaTiO_3$ and (**b**) epoxy/x phr $ZnTiO_3$ phr/5 phr $BaTiO_3$.

The effect of filler content on the IP and β- and γ-relaxations is shown in Figure 8. Figure 8a presents the loss tanδ at 160 °C versus frequency for the systems with a constant (5 phr) $ZnTiO_3$ content, varying the content of $BaTiO_3$. Recalling Figures 3, 4 and 5b, and since tanδ is defined as the ratio of the imaginary to the real part of dielectric permittivity, hybrid systems with high ε' exhibit relatively lower values of the IP peak, as shown in the inset of Figure 8a. In Figure 8b, the spectra of tanδ as a function of temperature at 10^6 Hz, for the same systems, clearly form two loss peaks corresponding, from low to high temperatures, to γ- and β-relaxation, respectively. As can be seen, the variation in the filler content does not influence these weak processes.

The dynamics of the recorded relaxation processes, for the hybrid systems, are presented in Figure 9a (constant $ZnTiO_3$ content and varying the $BaTiO_3$ content) and Figure 9b

(constant $BaTiO_3$ content and varying the $ZnTiO_3$ content). IP and γ-relaxation follow an Arrhenius type dependence on temperature, which can be expressed via Equation (1):

$$f_{max} = f_0 exp\left(-\frac{E_A}{k_B T}\right) \quad (1)$$

where f_{max} is the frequency where a loss peak occurs at temperature T, f_0 is a pro-exponential factor, E_A is the activation energy, and k_B is the Boltzmann constant. The obtained data did not allow a reliable fitting procedure to be performed for β-relaxation, and thus this process is omitted from Figure 9. The glass-to-rubber transition mode (α-relaxation) deviates from the Arrhenius behavior because of the variation in the free volume, being in accordance with the so-called Vogel–Fulcher–Tamann relation [28,29], which is expressed by Equation (2):

$$f_{max} = f_0 exp\left(-\frac{B}{T - T_V}\right) \quad (2)$$

where B is a temperature dependent factor which is considered as a measure of the activation energy and T_V is the ideal glass transition temperature or Vogel temperature. The obtained results by fitting the data via Equations (1) and (2) are listed in Table 1.

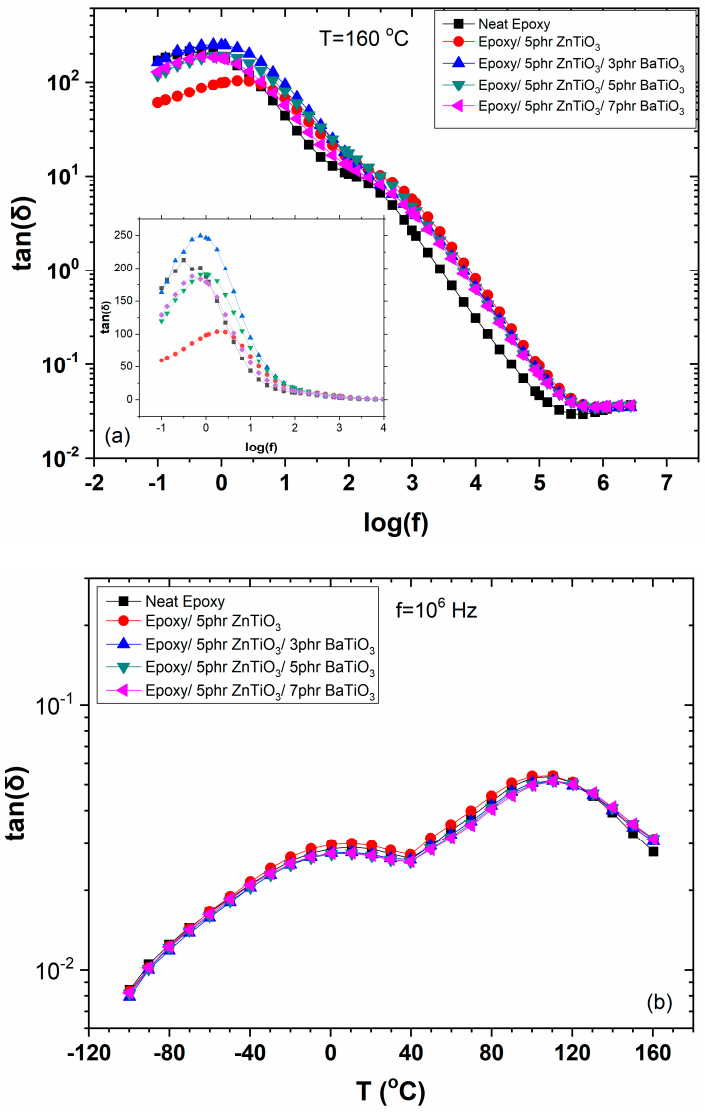

Figure 8. Loss tanδ for the epoxy/5 phr $ZnTiO_3$ phr/x phr $BaTiO_3$ nanocomposites versus (**a**) frequency at 160 °C and (**b**) temperature at 10^6 Hz.

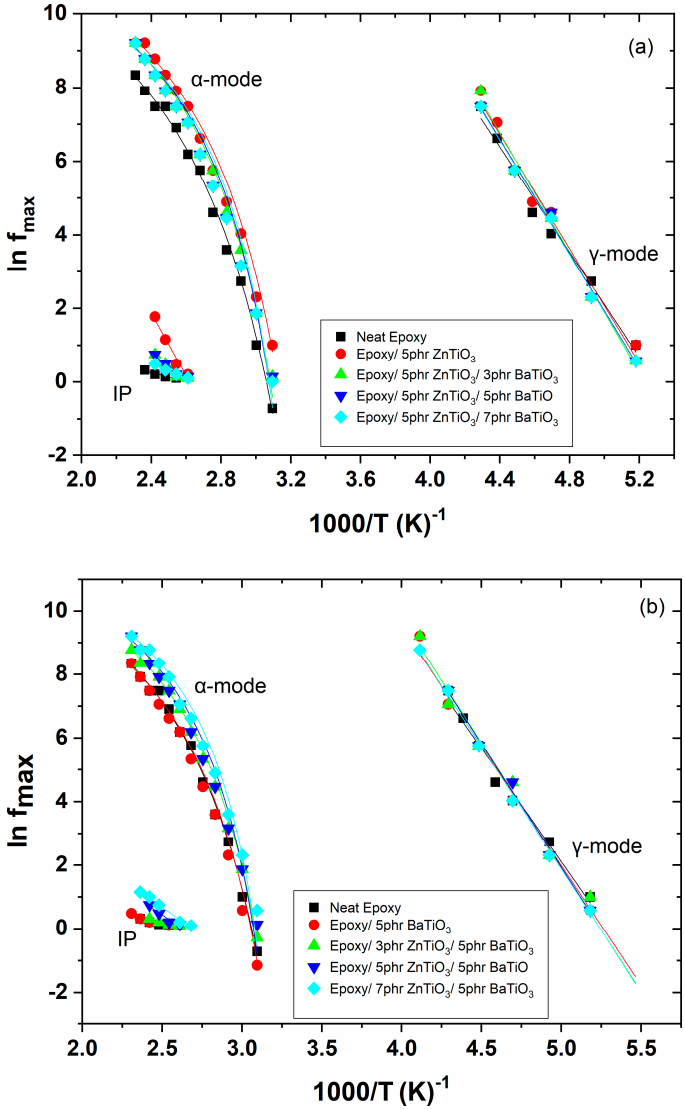

Figure 9. Relaxations loss peaks position as a function of reciprocal temperature for the nanocomposites: (**a**) epoxy/5 phr $ZnTiO_3$ phr/x phr $BaTiO_3$ and (**b**) epoxy/x phr $ZnTiO_3$ phr/5 phr $BaTiO_3$.

PNCs have been considered as suitable materials for energy storing and retrieving in fast charge/discharge processes, since the dispersed nanoparticles are acting as a distributed network of nanocapacitors. The studied hybrid PNCs were charged by applying two different levels of voltage (100 V and 200 V) for 60 s and then discharged (in the absence of an external voltage). During both procedures (charge/discharge), the current as a function of time was recorded, thus allowing for the evaluation of the stored and retrieved energy. The stored or retrieved energy can by calculated via Equation (3) [8,9,30]:

$$E = \frac{1}{2}\frac{Q^2}{C} = \frac{1}{2}\frac{[\int I(t)dt]^2}{C} \quad (3)$$

where E is the stored or retrieved energy at the hybrid nanocomposite, Q is the amount of charge, $I(t)$ is the charging or discharging current, and C is the capacitance of the nanocomposite. The latter is obtained by the dielectric data at the lowest measured frequency.

In Figure 10a,b, the stored and retrieved energies for hybrid nanocomposites, charged with 200 V, are depicted. In all cases, the stored and retrieved energy increases with the filler content. Interestingly, in the cases where the sum of the $ZnTiO_3$ and $BaTiO_3$ content is equal to 8 or 12 phr, the systems with a higher zinc titanate content (5 or 7 phr) exhibit the

bigger values of the stored/retrieved energy. The amounts of stored/retrieved energies also enhance with the increase in the charging voltage. Figure S6 presents relative data for the same systems shown in Figure 10, charged at 100 V. Figure 11 provides curves of the relative coefficient of energy efficiency for the nanocomposites presented in Figure 10. The relative coefficient of energy efficiency is defined according to Equation (4) and gives a direct comparison of the retrieved energy from the nanocomposites relatively to the retrieved energy from the unreinforced matrix [11,14]:

$$n_{rel} = \frac{E_{retr,\ comp}}{E_{retr,\ matrix}} \quad (4)$$

where $E_{retr,comp}$ and $E_{retr,matrix}$ are the retrieved energies from a nanocomposite and the neat matrix, respectively, under the same charging conditions. As can be seen in Figure 11, the recovered energy from the hybrid nanocomposites is several times higher than the corresponding one from the matrix. Optimum performance is shown by the system with 7 phr $ZnTiO_3$/5 phr $BaTiO_3$, which exhibits almost 30 times higher recovered energy than the matrix, in the whole examined period of time, and instantaneously exceeds 50 times the retrieved energy from the matrix.

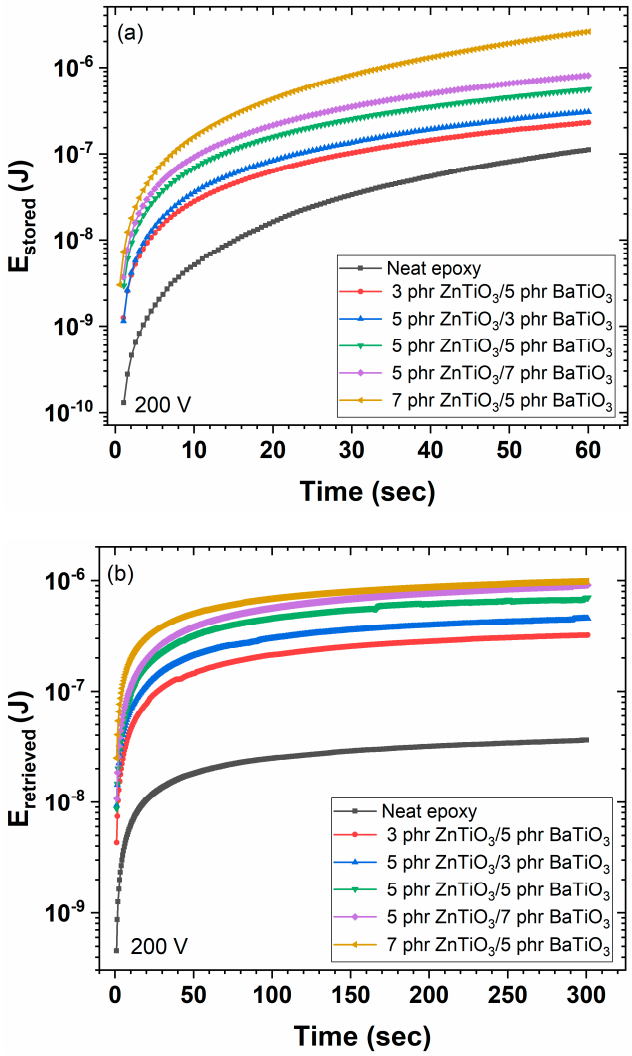

Figure 10. (**a**) Stored and (**b**) retrieved energy to the examined hybrid nanocomposites at 200 V charging voltage as a function of time.

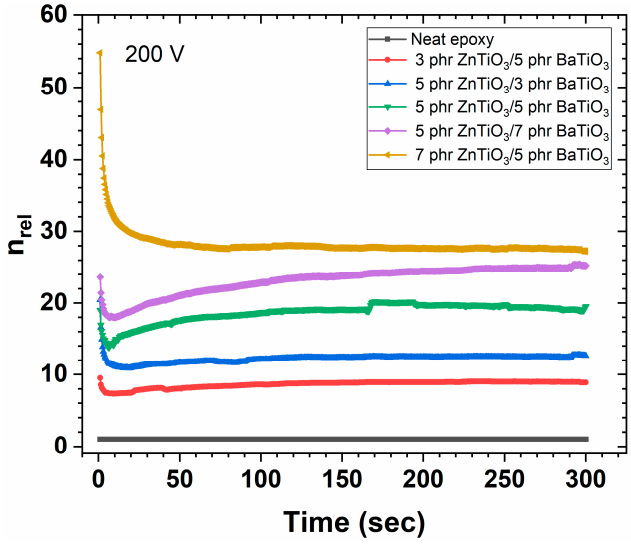

Figure 11. Relative coefficient of energy efficiency of the examined hybrid nanocomposites as a function of time.

The piezoelectric coefficient d_{33} quantifies the volume change when a piezoelectric material is subject to an electric field, or the generated polarization upon the application of mechanical stress. Figure 12 provides evidence for the effect of filler content ($ZnTiO_3$ or $BaTiO_3$, or both $ZnTiO_3$ and $BaTiO_3$) on the piezoelectric coefficient of the nanocomposites in ambient conditions. In the case of the binary nanocomposites (epoxy/$ZnTiO_3$ or epoxy/$BaTiO_3$), d_{33} increases with the piezoelectric phase content. By these means, the piezoelectric performance of zinc titanate, at room temperature, is apparent. The same behavior is observed in the hybrid nanocomposites (epoxy/ $ZnTiO_3$/$BaTiO_3$), although the resulting values for the d_{33} coefficient are remarkably higher, indicating a synergetic effect between the two reinforcing phases. The results from Figure 12 imply that the employed fillers can be exploited as piezoelectric nanogenerators and hybrid systems as sensing, activating, or energy converting structures.

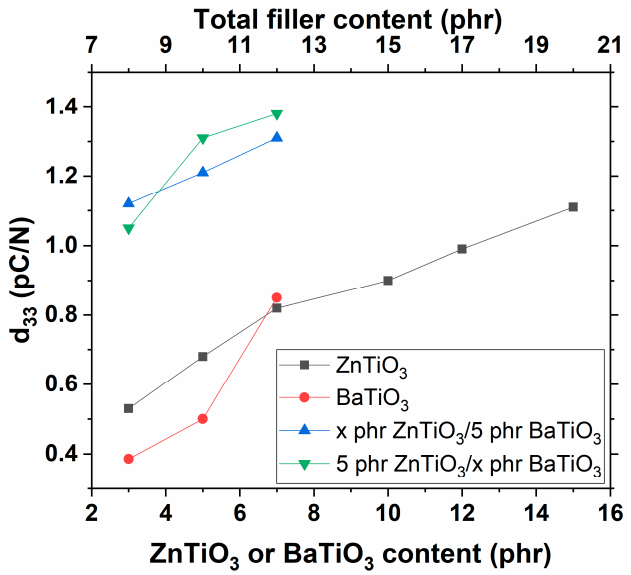

Figure 12. Piezoelectric coefficient as a function of filler content for binary and hybrid nanocomposites.

5. Conclusions

In the present study, nanocomposites of epoxy resin and ceramic particles of zinc titanate ($ZnTiO_3$) and barium titanate ($BaTiO_3$) were prepared at different concentrations of reinforcing phases. Structural (XRD patterns) and morphological (SEM images) studies revealed the successful fabrication of the nanocomposites and the fine distribution of the ceramic particles. The dielectric response and relaxation phenomena were investigated by means of Broadband Dielectric Spectroscopy (BDS). From the conducted analysis, it becomes evident that both the polymeric matrix and the reinforcing phase contribute to the recorded relaxation phenomena. Dielectric permittivity increases, in general, with ceramic nanoparticles content and temperature, while it decreases with frequency. At the highest $ZnTiO_3$ content, at a constant $BaTiO_3$ concentration, lower values of dielectric permittivity (ε') were observed, indicating the existence of an optimum content, different from the maximum one, which can be effectively dispersed in the polymer matrix. Hybrid nanocomposites exhibit at least four relaxation processes. At low frequencies and high temperatures, interfacial polarization phenomenon is present; at intermediate frequencies, α-mode due to the glass-to-rubber transition of the polymer is recorded; and finally, β- and γ- modes are recorded at low temperatures and high frequencies, resulting from the motion of polar side groups and local motion of small segments of the polymer chain. The ability of hybrid nanocomposites to store and retrieve energy was studied under dc conditions. Stored and retrieved energy increases with the charging voltage and filler content. Optimum performance was observed in the epoxy/7 phr $ZnTiO_3$/5 phr $BaTiO_3$ system, in which the recovered energy is almost 30 times higher than the corresponding one of the matrix and instantaneously exceeds 50 times the retrieved energy from the matrix. The piezoelectric response, as studied via the piezoelectric coefficient d_{33}, of the nanocomposites is significantly enhanced in the case of the hybrid systems, indicating a synergetic process between the fillers and their ability to act as piezoelectric nanogenerators.

Supplementary Materials: The following supporting information can be downloaded at: https://www.mdpi.com/article/10.3390/jcs8060225/s1, Figure S1: SEM image of a cryo-fractured cross-sectional surface for the epoxy/7 phr $ZnTiO_3$/7 phr $BaTiO_3$ nanocomposite at a lower magnification; Figure S2: (a) Real part of dielectric permittivity and (b) loss tanδ as a function of frequency and temperature for the neat epoxy; Figure S3: Real part of dielectric permittivity as a function of temperature, at 0.1 Hz for: (a) $ZnTiO_3$ nanoparticles (inset presents the same data at a narrower temperature range), and (b) hybrid nanocomposites and unreinforced matrix; Figure S4: Real part of dielectric permittivity as a function of frequency and temperature for the: (a) epoxy/12 phr $ZnTiO_3$, and (b) epoxy 12 phr $BaTiO_3$ nanocomposites; Figure S5: Imaginary part of electric modulus as a function of frequency at 50 °C for the nanocomposites: (a) epoxy/x phr $ZnTiO_3$ and (b) epoxy/x phr $BaTiO_3$; Figure S6: (a) Stored and (b) retrieved energy to the examined hybrid nanocomposites at 100 V charging voltage, as a function of time.

Author Contributions: For conceptualization, methodology, and validation A.C.P., E.I.K. and G.C.P. are responsible; formal analysis, investigation, and data curation, was conducted by A.C.P., E.I.K., O.V., G.N.M. and G.C.P.; writing—original draft preparation, A.C.P. and G.C.P.; writing—review and editing, A.C.P. and G.C.P.; supervision, and project administration G.C.P. All authors have read and agreed to the published version of the manuscript.

Funding: The present research was not funded by any external source.

Data Availability Statement: Data are available upon request.

Acknowledgments: Authors would like to acknowledge ICEHT-FORTH for providing access to XRD facilities.

Conflicts of Interest: The authors declare no conflicts of interest.

References

1. Friedrich, K. Routes for achieving multifunctionality in reinforced polymers and composite structures. In *Multifunctionality of Polymer Composites*; Friedrich, K., Breuer, U., Eds.; Elsevier: Amsterdam, The Netherlands, 2015; pp. 3–41, ISBN 978-0-323-26434-1.
2. Song, K.; Guo, J.Z.; Liu, C. *Polymer-Based Multifunctional Nanocomposites and Their Applications*; Elsevier: Amsterdam, The Netherlands, 2019; ISBN 9780128150672.
3. Zha, J.W.; Zheng, M.S.; Fan, B.H.; Dang, Z.M. Polymer-based dielectrics with high permittivity for electric energy storage: A review. *Nano Energy* **2021**, *89*, 106438. [CrossRef]
4. Vryonis, O.; Anastassopoulos, D.L.; Vradis, A.A.; Psarras, G.C. Dielectric response and molecular dynamics in epoxy-$BaSrTiO_3$ nanocomposites: Effect of nanofiller loading. *Polymer* **2016**, *95*, 82–90. [CrossRef]
5. Sanida, A.; Stavropoulos, S.G.; Speliotis, T.; Psarras, G.C. Development, characterization, energy storage and interface dielectric properties in $SrFe_{12}O_{19}$/epoxy nanocomposites. *Polymer* **2017**, *120*, 73–81. [CrossRef]
6. Koufakis, E.; Mathioudakis, G.N.; Patsidis, A.C.; Psarras, G.C. $ZnTiO_3$/epoxy resin nanocomposites: Development, dielectric behaviour and functionality. *Polym. Test.* **2019**, *77*, 105870. [CrossRef]
7. Sanida, A.; Stavropoulos, S.G.; Speliotis, T.; Psarras, G.C. Investigating the Effect of Zn Ferrite Nanoparticles on the Thermomechanical, Dielectric and Magnetic Properties of Polymer Nanocomposites. *Materials* **2019**, *12*, 3015. [CrossRef] [PubMed]
8. Manika, G.C.; Psarras, G.C. Barium titanate/epoxy resin composite nanodielectrics as compact capacitive energy storing systems. *Express Polym. Lett.* **2019**, *13*, 749–758. [CrossRef]
9. Manika, G.C.; Psarras, G.C. $SrTiO_3$/Epoxy Nanodielectrics as Bulk Energy Storage and Harvesting Systems: The Role of Conductivity. *ACS Appl. Energy Mater.* **2020**, *3*, 831–842. [CrossRef]
10. Bafakeeh, O.T.; Shewakh, W.M.; Abu-Oqail, A.; Abd-Elaziem, W.; Ghafaar, M.A.; Bakafeeh, M.A.-O. Synthesis and Characterization of Hybrid Fiber-Reinforced Polymer by Adding Ceramic Nanoparticles for Aeronautical Structural Applications. *Polymers* **2021**, *13*, 4116. [CrossRef]
11. Gioti, S.; Sanida, A.; Mathioudakis, G.N.; Patsidis, A.C.; Speliotis, T.; Psarras, G.C. Multitasking Performance of Fe_3O_4/$BaTiO_3$/Epoxy Resin Hybrid Nanocomposites. *Materials* **2022**, *15*, 1784. [CrossRef]
12. Vikulova, M.; Nikityuk, T.; Artyukhov, D.; Tsyganov, A.; Bainyashev, A.; Burmistrov, I.; Gorshkov, N. High-k Three-Phase Epoxy/$K_{1.6}(Ni_{0.8}Ti7_{.2})O_{16}$/CNT Composites with Synergetic Effect. *Polymers* **2022**, *14*, 448. [CrossRef]
13. Blatsi, C.; Patsidis, A.C.; Psarras, G.C. Dielectric Properties and Energy Storage of Hybrid/Boron Nitride/Titanium Carbide/Epoxy Nanocomposites. *J. Compos. Sci.* **2022**, *6*, 259. [CrossRef]
14. Manika, G.C.; Gioti, S.; Sanida, A.; Mathioudakis, G.N.; Abazi, A.; Speliotis, T.; Patsidis, A.C.; Psarras, G.C. Multifunctional Performance of Hybrid $SrFe_{12}O_{19}$/$BaTiO_3$/Epoxy Resin Nanocomposites. *Polymers* **2022**, *14*, 4817. [CrossRef] [PubMed]
15. Xu, W.; Wang, Z.; Cao, H.; Zhou, L.; Jiang, N.; Ke, K.; Liu, Z.; Yang, W.; Yang, M. Optimization of the Thermally Conductive Low-*k* Polymer Dielectrics Based on Multisource Free-Volume Effects. *ACS Appl. Mater. Interfaces* **2024**, *16*, 16809–16819. [CrossRef] [PubMed]
16. Patsidis, A.C.; Psarras, G.C. Structural transition, dielectric properties and functionality in epoxy resin—Barium titanate nanocomposites. *Smart Mater. Struct.* **2013**, *22*, 115006. [CrossRef]
17. Manika, G.C.; Andrikopoulos, K.S.; Psarras, G.C. On the Ferroelectric to Paraelectric Structural Transition of $BaTiO_3$ Micro/Nanoparticles and Their Epoxy Nanocomposites. *Molecules* **2020**, *25*, 2686. [CrossRef] [PubMed]
18. Chávez, E.; Fuentes, S.; Zarate, R.A.; Padilla-Campos, L. Structural analysis of nanocrystalline $BaTiO_3$. *J. Mol. Struct.* **2010**, *984*, 131–136. [CrossRef]
19. Ben Belgacem, R.; Chaari, M.; Matoussi, A. Studies on structural and electrical properties of ZnO/TiO_2 composite materials. *J. Alloys Compd.* **2015**, *651*, 49–58. [CrossRef]
20. Wattanawikkam, C.; Pecharapa, W. Sonochemical synthesis, characterization, and photocatalytic activity of perovskite $ZnTiO_3$ nanopowders. *IEEE Trans. Ultrason. Ferroelectr. Freq. Control.* **2016**, *63*, 1663–1667. [CrossRef]
21. Ben Belgacem, R.; Chaari, M.; Braña, A.F.; Garcia, B.J.; Matoussi, A. Structural, electric modulus and complex impedance analysis of ZnO/TiO_2 composite ceramics. *J. Am. Ceram. Soc.* **2017**, *100*, 2045–2058. [CrossRef]
22. Chang, Y.-S.; Chang, Y.-H.; Chen, I.-G.; Chen, G.-J.; Chai, Y.-L.; Fang, T.-H.; Wu, S. Synthesis, formation and characterization of $ZnTiO_3$ ceramics. *Ceram. Int.* **2004**, *30*, 2183–2189. [CrossRef]
23. Barman, S.; Paul, S.; Ranjan, P.; Das, S.; Datta, A. Emerging ferroelectricity and piezoelectric energy harvesting properties in lead-free zinc titanate nanocrystals. *J. Mater. Sci.* **2023**, *58*, 7060–7075. [CrossRef]
24. Meisak, D.; Kinka, M.; Plyushch, A.; Macutkevič, J.; Zarkov, A.; Schaefer, S.; Selskis, A.; Samulionis, V.; Kuzhir, P.; Banys, J.; et al. Piezoelectric Nanogenerators Based On $BaTiO_3$ PDMS Composites for High-Frequency Applications. *ACS Omega* **2023**, *8*, 13911–13919. [CrossRef]
25. *ASTM D150-18*; Standard Test Methods for AC Loss Characteristics and Permittivity (Dielectric Constant) of Solid Electrical Insulation. American Society for Testing Materials, ASTM International: West Conshohocken, PA, USA, 2018.
26. *ASTM D257-14*; Standard Test Methods for DC Resistance or Conductance of Insulating Materials. American Society for Testing Materials, ASTM International: West Conshohocken, PA, USA, 2021.
27. Patsidis, A.; Psarras, G.C. Dielectric behaviour and functionality of polymer matrix—Ceramic $BaTiO_3$ composites. *Express Polym. Lett.* **2008**, *2*, 718–726. [CrossRef]

28. Psarras, G.C. Conductivity and dielectric characterization of polymer nanocomposites. In *Physical Properties and Applications of Polymer Nanocomposites*; Tjong, S.C., Mai, Y.-W., Eds.; Woodhead Publishing: Cambridge, MA, USA, 2010; pp. 31–69, ISBN 9781845696726.
29. Psarras, G.C. Fundamentals of dielectric theories. In *Dielectric Polymer Materials for High-Density Energy Storage*; Dang, Z.M., Ed.; Elsevier Inc.: Cambridge, UK, 2018; pp. 11–57.
30. Manika, G.C.; Psarras, G.C. Energy storage and harvesting epoxy nanodielectrics in $BaTiO_3$. *High Volt.* **2016**, *1*, 151–157. [CrossRef]